DURABILITY STUDY OF THE AISI 1024HR AND AISI 304HR ALLOYS APPLIED IN THE ORGANIC WASTE INDUSTRY

ESTUDO DE DURABILIDADE DOS AÇOS LAMINADOS A QUENTE AISI 1024 E AISI 304 APLICADOS NA INDÚSTRIA DE TRATAMENTO DE LIXOS ORGÂNICOS

Teresa Morgado[1,2,3], Ricardo Paulo[4], Pedro Amaral[4], Mário Pereira[5], José Simões[6], Alexandre Velhinho[7,8]

[1]LNEC- Laboratório de Engenharia Civil, Lisboa, Portugal; email: t.morgado@lnec.pt
[2]UNIDEMI, Universidade Nova de Lisboa, Portugal; email: t.morgado@fct.unl.pt
[3]IPT- Polytechnic Institute of Tomar, Portugal; email: t.morgado@ipt.pt
[4]DEMI, FCT NOVA; email: r.paulo@campus.fct.unl.pt; pm.amaral@campus.fct.unl.pt
[5]ESTG/, Polytechnic Institute of Leiria, Portugal; email: mario.pereira@ipleiria.pt
[6]ESTS/IPS – Polytechnic Institute of Setúbal, Portugal; email: jose.simoes@ests.ips.pt
[7]DCM/FCTUNL, FCT NOVA; email: ajv@fct.unl.pt
[8]CENIMAT/ FCTUNL, FCT NOVA; email: ajv@fct.unl.pt



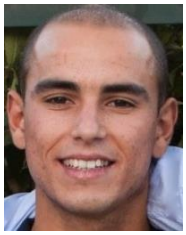


ABSTRACT

This paper studies the durability of hot rolled steel alloys, AISI 1024 and AISI 304, considering their application in components of the solid waste industry. Through the analyse of the intrinsic manufacturing defects, microhardness and fatigue study with and without corrosion results, is presented a new approach to determine the durability of two steel alloys based on fatigue limit stress prediction models. For the study of the effect of the corrosion the test specimens to obtain the S-N curves were submitted to organic waste for 48 hours.

Keywords: Durability, S-N Curves, manufacturing defects, fatigue limit stress prediction models, AISI 1024HR, AISI 304HR, organic waste industry

RESUMO

Este artigo estuda a durabilidade das ligas de aço laminado a quente, AISI 1024 e AISI 304, tendo em conta a sua aplicação em componentes da indústria de resíduos sólidos. Através do estudo dos defeitos intrínsecos de fabrico, da microdureza Vicker do material e dos resultados do estudo de fadiga sem e com corrosão apresenta-se uma nova metodologia para determinar a durabilidade das duas ligas de aço baseada em modelos de previsão de tensão limite de fadiga. Para o estudo do efeito da corrosão, os provetes usados para obtenção das curvas S-N, foram submetidos em lixo orgânico durante 48 horas.

1. INTRODUCTION

The presence of intrinsic manufacturing defects, the service loads, the service environment, the mechanical proprieties are important factors that affect the durability of mechanical components (Morgado, 2015). The presence of manufacturing defects in the materials leads to failures at much lower applied stresses. It is therefore of primary

importance to consider such defect features as input parameters in fatigue limit assessment.

The fatigue limit stress prediction models make possible to determine the durability of metals, considering experimental fatigue tests, mechanical properties, hardness, manufacturing technology (namely through intrinsic defects in the process), empirical constants depending on the manufacturing processes and components dimension (Morgado, 2013).

Murakami and co-workers (1994, 2001, 2012) have investigated the effects of defects, inclusions, and inhomogeneities on fatigue strength of high strength steels, and expressed the fatigue limit (σ_{FL}) as a function of Vickers hardness (HV) and the square root of the projection area of an inclusion or small defect (equation 1). This model is known as Murakami-Endo model.

$$\sigma_{LF} = C\frac{(HV+120)}{(\sqrt{area})^{1/6}} \times \left(\frac{1-R}{2}\right)^{\alpha} \quad (1)$$

where C value depends of the manufacturing defect position (C=1.56 for intern defect and C=1.43 for superficial defects). The stress ratio is given by R and $\alpha = 0.226 + HV \times 10^{-4}$.

Bathias and Paris (Bathias, 2005) had considered a new empirical formula that includes the number of cycles (equation 2).

$$\sigma_{LF} = \beta\frac{(HV+120)}{(\sqrt{area})^{1/6}} \times \left(\frac{1-R}{2}\right)^{\alpha} \quad (2)$$

where β value depends of the number of cycles, N, and of the position of the manufacturing defects, this is, for internal defects uses the empirical expression $\beta = 3.09 - 0.12lnN$ and for superficial defects $\beta = 2.79 - 0.108lnN$.

Morgado and Sousa e Brito (Morgado, 2013) presented a study of the influence of casting defects on the fatigue limit of a cast steel ASTM A148 90-60 of a railway component. The results of two models, Murakami-Endo and Bathias-Paris, to predict strength show the effect of the non-metallic inclusions, porosities and shrinkage cavities inside and at surface, in the fatigue strength. In a general way, the Bathias-Paris model presents a lower error percentage in relation to experimental stress than the ones that Murakami model presents; although for some specimens it presents higher values. Both the models present error values lower of 0.5%.

Paulo R. and Morgado (Paulo, 2018) studied the wear behavior of three rolled steels (AISI 1024, AISI P20 and AISI 304) for the production of a worm screw applied to the organic waste treatment industry, that presented a few weeks of life service. This component is, also, subjected to corrosion and fatigue. From the conclusions of that work, the AISI 1024HR and the AISI 304HR are recommended for produce the screw to move organic waste.

Continuing Paulo and Morgado works (Paulo, 2018), in this work, the authors present a new approach to predict the durability of AISI 1024HR and AISI304HR. The methodology used is based on experimental work that was divided in four phases: the manufacturing and preparation of the samples and specimens according to standard recommendations, the manufacturing defects study, the Vickers hardness study and the fatigue with and without corrosion study. The algorithm to predict the durability is based on the experimental results obtained and, on the Murakami-Endo and Bathias-Paris models.

2. MATERIALS AND EXPERIMENTAL PROCEDURE

In table 1 is presented the chemical composition of the hot rolled steels AISI 1024HR and the AISI 304HR, objects of this study.

As described in the introduction, to obtain the fatigue limit stress values using Murakami-Endo (Murakami, 1994) and Bathias-Paris models (Bathias, 2005) it is necessary to determine the hardness of each material as well as the area of internal or superficial defects. The preparation of samples for the hardness test and for the manufacturing defects study was performed according to the ASTM standard (ASTM E3-11(2017)). To determine the hardness of both materials, the Vickers micro indentation hardness tests were conducted following the ASTM standard (ASTM E384-17).

Table 1 - Chemical composition

	C (%)	Si (%)	Mn (%)	Cu (%)	Ni (%)	Cr (%)	P (%)	S (%)
AISI 1024	0.22	0.55	1.60	0.55	-	-	0.03	0.03
AISI 304	0.07	10.0	2.00	-	10.50	17.50 -19.50	0.05	0.03

Twenty-eight specimens were prepared, fourteen samples of each material were used (nine samples for hardness determination and five samples for manufacturing defects study).

Before performing the fatigue tests with and without corrosion, a test specimen with specifications according to ASTM standard (ASTM E8/E8M-16a) was designed. Sixty-four test specimens of each material were used to obtain the SN curves. In fig. 1 is presented the geometry of the fatigue test specimen.

In order to analyze corrosion behavior of AISI1024 and AISI304 when submerged in an organic residue solution (lemon, potato and egg) three specimens of each material were immerse during 48 hours with a pH of 5 in the solution (see figure 2). Posteriorly a microscopic analysis was carried out to confirm the corrosion present at the specimens (see figures 3 and 4). As was expected, the AISI 1024HR presents more and biggest zones of corrosion. Nevertheless, AISI 304HR also presents pitting corrosion zones.

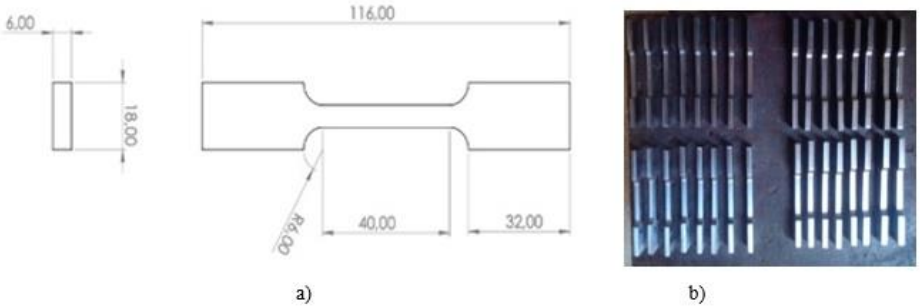

Fig. 1 - Fatigue test specimen: a) dimensions according to the standard (ASTM E8/E8M:16) a) AISI 304 test specimens for fatigue test without corrosion

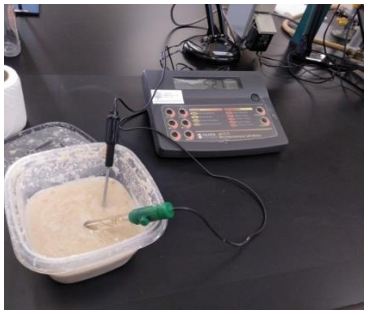

Fig. 2 - Organic residue solution composed by lemon, potato and eggs used to create corrosion

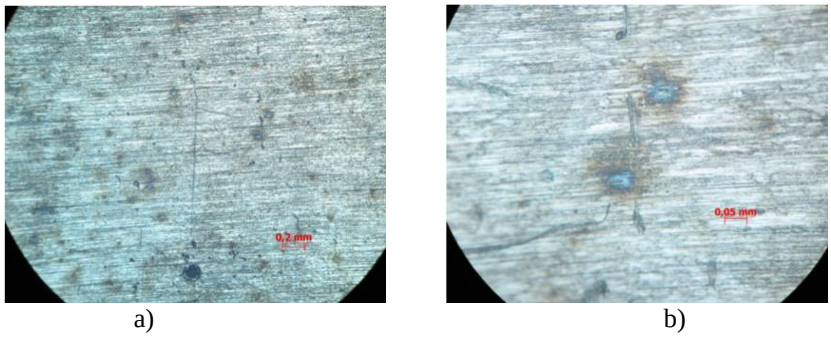

Fig. 3 - Microscopic observation of organic pitting corrosion on AISI1024 HR specimens after being submerce in a organic residue solution: a) magnification 5x b) magnification 20x

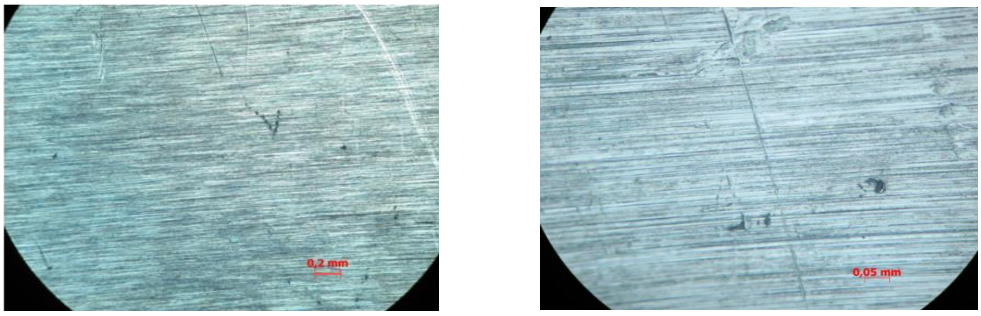

a) b)

Fig. 4 - Microscopic observation of organic pitting corrosion on AISI304 HR specimens after being submerce in organic residue solution: a) magnification 5x b) magnification 20x

2.1. Hardness test

Through the remaining material coming from the production phase of specimens, a cut was made using a mechanical saw to obtain the samples to hardness tests and manufacturing defects study. A resin and a hardener were mixed and after its solidification, formed samples were obtained. The polishing process was carried out, through an automatic rotation equipment and the successive application of abrasive sandpaper sequence: 80, 240, 320, 400, 600 and 1200 and 2500. Finally, the samples were subjected to polishing with a specific cloth and 1 µm diamond paste. This proceeding followed the ASTM standard (E3-11 (2017)).

Subsequently, the methodology performed in the micro indentation test, took into consideration the specifications of the ASTM standard (E384-17). A spacing of 0.5 mm was used between each indentation, thus ensuring a minimum distance of 2.5 times greater than the *Vickers* diagonal, using a test load of 500 g.f and with a duration of 10 seconds in each test. Ten indentations were made in each specimen.

Software Minitab was used to verify if the results obtained followed a normal distribution, as required in ASTM standard (ASTM 384-17). Probability plots were made using the Anderson-Darling test, in which the p-value must be equal or higher than the confidence value $\alpha = 0.05$. Figure 5 presents one of the probability graph for the AISI 1024-T-A sample.

2.2. Manufacturing defects analysis

For the defect material analysis, each sample was placed in an inverted optical microscope Leica DMI5000 M, whose software allowed

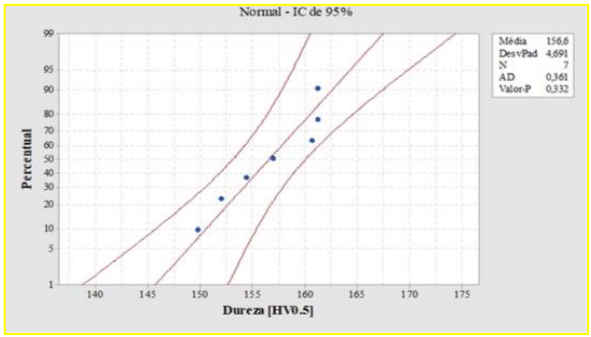

Fig. 5 - AISI 1024-T-A sample probability chart

to take multiple pictures along the specimen as shown in figure 6 (a) and (b). Once every image was obtained, as shown in figure 6 (c) and (d), they were subjected to threshold by ImageJ software to evidence defects (defects are shown in black). Finally, another tool from ImageJ software was used to count defects and measure their corresponding area.

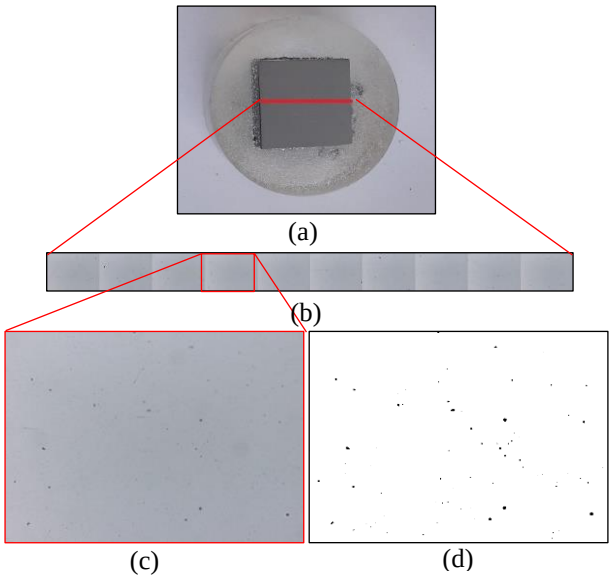

Fig. 6 – Sequence used to analyse defects: (a) direction of pictures identified; (b) multiple pictures taken; (c) original picture and (d) image with threshold

2.3. Fatigue testing

The fatigue tests were carried out using the universal servo-hydraulic equipment of mechanical tests *Instron 8802* (see Figure 7 a)). Its system has a maximum load capacity of up to 100 kN. For the implementation and acquisition of test data, the associated *Instron 880*0 controller and a computer with the *Instron SAX V7.0* software was used (see Figure 7 b)).

In the execution of the tests, a sinusoidal wave was used, with constant amplitude and stress ratio of R=0.05. It was also applied a frequency f= 10 Hz during each test. It was considered a room temperature of 25ºC.

S-N curves were obtained with four levels and the infinite life considered was a million of cycles.

3. RESULTS AND DISCUSSION

The hardness tests showed consistency with the values obtained along the samples. The average Vickers hardness results for AISI1024HR steel was 157HV and for AISI304HR was 160HV.

From the manufacturing defects study, was observed that AISI 1024 steel samples present a higher number of defects, and the largest defect presented an area of 2.2E-04 mm ^{2}; and for the AISI 304 stainless steel samples the defect in the upper area showed a value of 3.0E-03 mm^2.

In figure 8 is showed the areas defect distribution by classes, where A, B, C, D and E, correspond to defects areas classes between [0; 1.00×10^{-7}] mm^2, [1.00×10^{-7};1.00×10^{-6}] mm^2,

a) b)

Fig. 7 - Fatigue Testing Experimental Layout: a) Universal servo-hydraulic equipment *Instron 8802; b) Instron 880*0 controller and the computer with the *Instron SAX V7.0* software

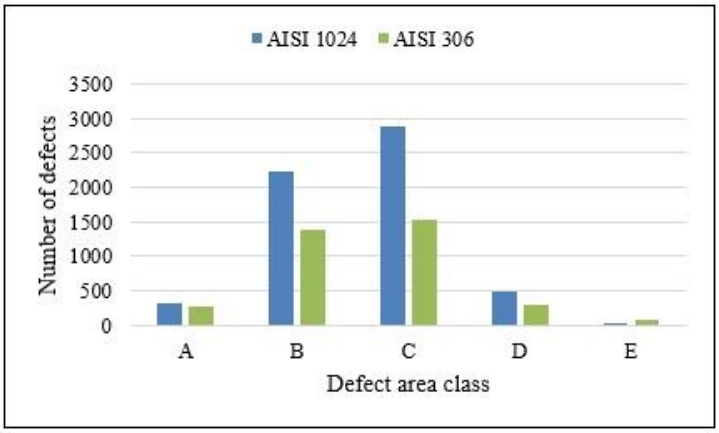

Fig. 8 – Defect distribution by area classes.

$[1.00 \times 10^{-6}; 1.00\times10^{-5}]$ mm^2, $[1.00 \times 10^{-5}; 1.00 \times 10^{-4}]$ mm^2 and $[1.00 \times 10^{-4};+\infty]$ mm^2, respectively.

With fatigue tests were obtained the S-N curves for both materials subject to fatigue and fatigue under corrosion. These results are shown in the Figure 9 and Figure 10, for AISI1024HR and AISI 304HR, respectively.

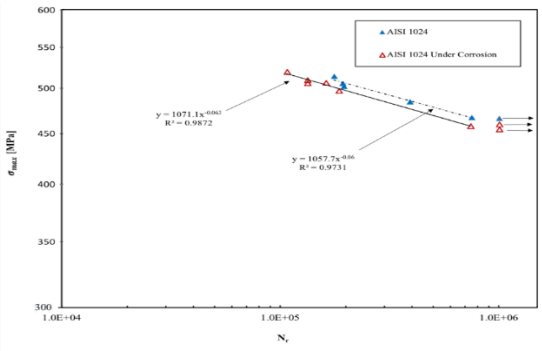

Fig. 9 - AISI 1024HR S-N curves subjected to fatigue and fatigue under corrosion conditions

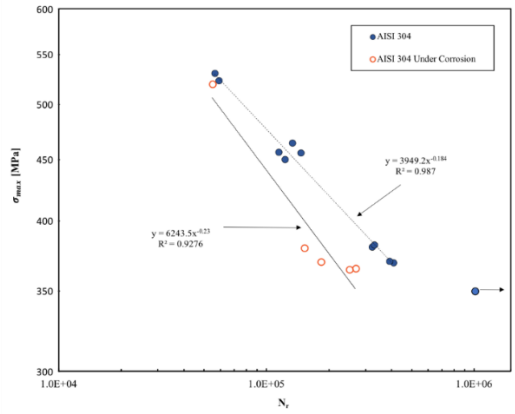

Fig. 10 - AISI 304HR S-N curves subjected to fatigue and fatigue under corrosion conditions

With the quantification of defect areas obtained as well as the determination of hardness values for both materials, it was developed a new approach to calculate the durability based on experimental SN curves and on Murakami-Endo and Bathias-Paris models. In Figure 11 it is presented the durability results considering the SN curves showed in figures 9 and 10 and both prediction fatigue limits models. As can be observed in Figure 11, the manufacturing defect position (Int – Internal and Sup – Superficial) and the fatigue conditions influence significatively the durability; and presents a finite life in high cycle fatigue regime. The highest durability values are observed for AISI 304HR independently of the fatigue conditions. Durability values based on Murakami-Endo model present the most conservative values. For AISI 1024HR, independently of the model and fatigue conditions, the cycles number supported by the material is lower than $12.9\text{x}10^3$ cycles. The durability highest values are presented in AISI 304HR, when internal manufacturing defects and Bathias-Endo Model are considered.

4. CONCLUSION

From this study it is concluded that, on average, the durability for both materials, AISI1024HR and AISI 304HR steels, obtained through the Murakami-Endo model, decreases 14% when considering the fatigue under corrosion in relation to the simple fatigue.

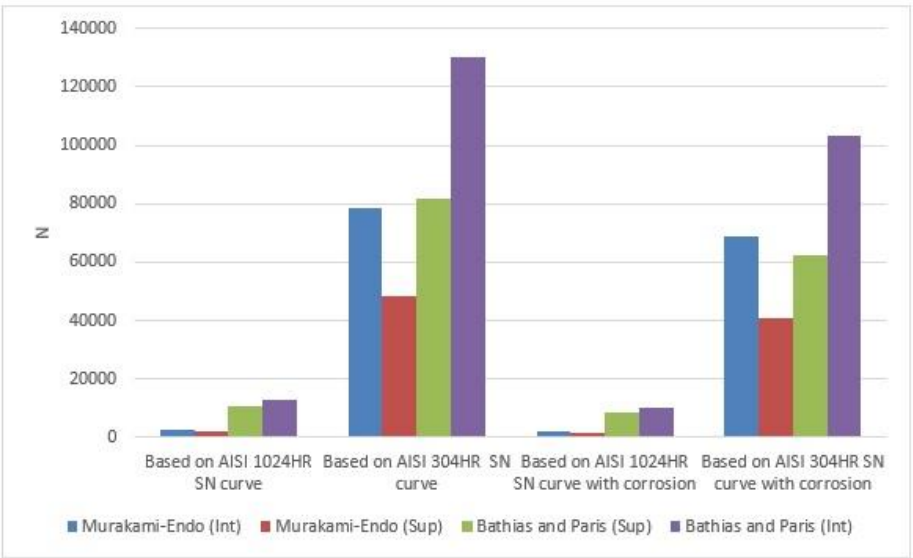

Fig. 11 –AISI 1024HR and AISI 304HR durability considering fatigue and fatigue under corrosion conditions

Through the Bathias- Paris model durability values have decreased 18% for AISI 1024HR steel and 20% for AISI 304HR stainless steel.

Considering the position of the surface intrinsic manufacturing defects in relation to the internal ones, it can be concluded that the durability for both steels decreases significantly regardless of the prediction model and the S-N curve considered. The decrease in the average durability of AISI 1024HR steel, considering the position of the manufacturing defect is 20% with Murakami-Endo model and 17% with Bathias-Paris model. And, for AISI 304HR material the durability decrease is of 40% and 38% considering, respectively, the Murakami-Endo and Bathias-Paris models.

Both materials presented a finite life durability in a high cycle fatigue regime independently of the manufacturing defect position fatigue and fatigue under organic corrosion condition.

From this new approach proposed to calculate the durability it is concluded that the influence of the manufacturing defect position considering fatigue under different environment conditions, depends significantly of the material and of the fatigue limit prediction model. And is concluded that the AISI 304HR is the most sensibility to that influences, nevertheless, presents the highest values of durability.

ACKNOWLEDGMENTS

The authors from FCT NOVA would like to acknowledge Fundação para a Ciência e Tecnologia (FCT, I.P.) for financial support via Pest-OE/EME/UI0667/2014 and LA25-2013-2014.

REFERENCES

Bathias C., Paris P. C. (2005). Gigacycle Fatigue in Mechanical Practice. Series Dekker Mechanical Engineering (Book 185). Publisher: CRC Press. ISBN-10: 0-8247-2313-9.

Morgado T. (2015). Failure of steel coupling used in railway transport. Handbook of Materials Failure Analysis with Case Studies from the Aerospace and Automotive Industries, chapter 20. Edited by Abdel Salam Hamdy Makhlouf *and* Mahmood Aliofkhazraei. Elsevier BH. Published: UK2016. Pp449-469. ISBN 978-0-12-800950-5. eBook ISBN: 9780128011775. First online: 24*th* August 2015: https://www.elsevier.com/books/handbook-of-materials-failure-analysis-with-case-studies-from-the-aerospace-and-automotive-industries/makhlouf/978-0-12-800950-5

Morgado T. L. M., Brito A.S. (2013). Study of casting defects and fatigue limit models of a railway component. Thirteenth International ASTM/ESIS Symposium on Fatigue and Fracture Mechanics (39th National Symposium on Fatigue and Fracture Mechanics), November 13-15, 2013.

Murakami Y, Endo M. (1994). Effects of defects, inclusions and inhomogeneities on fatigue strength. Int J Fatigue; 16(3):163-182. https://doi.org/10.1016/0142-1123(94)90001-9

Murakami Y, Nomoto T, Ueda T. (2001). Factors influencing the mechanism of superlong fatigue failure in steels. Fatigue Fract Eng Mater Struct 2001;22:581–90. https://doi.org/10.1046/j.1460-2695.1999.00187.x

Murakami Y. (2012). Metal fatigue: effect of small defects and nonmetallic inclusions. Elsevier Science. ISBN: 978-0-08-044064-4. eBook ISBN: 9780080496566. https://www.elsevier.com/books/metal-fatigue-effects-of-small-defects-and-nonmetallic-inclusions/murakami/978-0-08-044064-4

Paulo R. and Morgado T.. (2018). Wear Behaviour of AISI 1024, AISI P20 and AISI 304 hot rolled teels used in organic waste treatment industry. Revista da Associação Portuguesa de Análise Experimental de Tensões, Mecânica Experimental, vol. 30, pp 55-60. http://www-ext.lnec.pt/APAET/pdf/Rev_30_A7.pdf

ASTM E3-11 (2017). Standard Practice for Preparation of Metallographic Specimens. ASTM International, West Conshohocken, PA, 2017. DOI: 10.1520/E0003-11R17. https://www.astm.org/Standards/E3.html

ASTM E384-17. Standard Test Method for Microindentation Hardness of Materials. ASTM International, West Conshohocken, PA, 2017. DOI: 10.1520/E0384-17. https://www.astm.org/Standars/E384.html

ASTM E8/E8M-16a. Standard Test Methods for Tension Testing of Metallic Materials. ASTM International, West Conshohocken, PA, 2016. DOI: 10.1520/E0008_0008M-16A. https://www.astm.org/Standars/E8.html